Journal of Alloys and Compounds 509 (2011) 6737–6750

Contents lists available at ScienceDirect

Journal of Alloys and Compounds

journal homepage: www.elsevier.com/locate/jallcom

Effect of increasing tellurium content on the electronic and optical properties of cadmium selenide telluride alloys $CdSe_{1-x}Te_x$: An *ab initio* study

Ali Hussain Reshak[a,b,*], I.V. Kityk[c], R. Khenata[d,e], S. Auluck[f]

[a] *Institute of Physical Biology-South Bohemia University, Nove Hrady 37333, Czech Republic*
[b] *School of Material Engineering, Malaysia University of Perlis, P.O Box 77, d/a Pejabat Pos Besar, 01007 Kangar, Perlis, Malaysia*
[c] *Electrical Engineering Department, Technical University of Czestochowa, Al. Armii Krajowej 17/19, Czestochowa, Poland*
[d] *Laboratoire de Physique Quantique et de Modélisation Mathématique de la Matière (LPQ3 M), université de Mascara, Mascara 29000, Algeria*
[e] *Department of Physics and Astronomy, King Saud University, P.O. Box 2455, Riyadh 11451, Saudi Arabia*
[f] *National Physical Laboratory Dr. K S Krishnan Marg, New Delhi 110012, India*

ARTICLE INFO

Article history:
Received 26 September 2010
Received in revised form 13 January 2011
Accepted 5 March 2011
Available online 16 March 2011

Keywords:
Optical properties (linear and nonlinear)
DFT
FPLAPW

ABSTRACT

An all electron full potential linearized augmented plane wave method, within a framework of GGA (EV-GGA) approach, has been used for an *ab initio* theoretical study of the effect of increasing tellurium content on the band structure, density of states, and the spectral features of the linear and nonlinear optical susceptibilities of the cadmium–selenide–telluride ternary alloys $CdSe_{1-x}Te_x$ (x = 0.0, 0.25, 0.5, 0.75 and 1.0). Our calculations show that increasing Te content leads to a decrease in the energy band gap. We find that the band gaps are 0.95 (1.76), 0.89 (1.65), 0.83 (1.56), 0.79 (1.44) and 0.76 (1.31) eV for x = 0.0, 0.25, 0.5, 0.75 and 1.0 in the cubic structure. As these alloys are known to have a wurtzite structure for x less than 0.25, the energy gaps are 0.8 (1.6) eV and 0.7 (1.55) eV for the wurtzite structure (x = 0.0, 0.25) for the GGA (EV-GGA) exchange correlation potentials. This reduction in the energy gaps enhances the functionality of the $CdSe_{1-x}Te_x$ alloys, at least for these concentrations, leading to an increase in the effective second-order susceptibility coefficients from 16.75 pm/V (CdSe) to 18.85 pm/V ($CdSe_{0.75}Te_{0.25}$), 27.23 pm/V ($CdSe_{0.5}Te_{0.5}$), 32.25 pm/V ($CdSe_{0.25}Te_{0.75}$), and 37.70 pm/V (CdTe) for the cubic structure and from 12.65 pm/V (CdSe) to 21.11 pm/V ($CdSe_{0.75}Te_{0.25}$) in the wurtzite structure. We find a nonlinear relationship between the absorption/emission energies and composition, and a significant enhancement of the electronic properties as a function of tellurium concentration. This variation will help in designing better second-order susceptibility materials by manipulating of the electronic structures of these materials with different compositions to achieve more delocalized atomic bonds.

1. Introduction

Investigation of the electronic band structure of II–VI semiconductor compounds has recently become an area of great activity. The reason for this is the possibility of fabrication of novel materials with adjustable electronic and magnetic properties. The II–VI compounds are of particular interest. In particular they provide us with core states which are accessible to calculations. The Cd-d states are 8–10 eV below the top of valence band [1]. The increasing activity and realization of the enormous potential for technological applications in the area of nonlinear optics (NLO), ranging from optical communications and computing to improve solid state laser systems, has recently heightened interest in this problem. The ternary cadmium–selenide–telluride quantum dots have been used as constant size biolables with tunable fluorescence emission in the far-red and near-infrared (650–850 nm) spectral range [2]. Das [3] used the $CdSe_{1-x}Te_x$ alloys to study the principal requirements of a good thin film photoelectrode for high efficiency photoelectrochemical (PEC) cells. The low resistivity and large grain size were found as the main requirements. The large size grains lead to a reduction of the grain boundary area of the thin films, with important consequences for efficient energy conversion. The low resistivity of the photoelectrodes is required to minimize the series resistance of the PEC cell which leads to lower short circuit current. Ravichandran et al. [4] prepared thin films of $CdSe_{1-x}Te_x$ using electro-deposition with varying doping concentrations of Te and studied the photoconductivity as a function of applied dc-electric field, time, wavelength, and the intensity of incident light at room temperature. More et al. [5] reported information pertaining to the chemo-synthesis of CdSe/CdTe thin films of variable composition which has been brought about with the objectives to study the deposition history, growth kinetics and the structural and opti-

* Corresponding author at: Institute of Physical Biology-South Bohemia University, Nove Hrady 37333, Czech Republic. Tel.: +420 777 729583; fax: +420 386 361231.
E-mail address: maalidph@yahoo.co.uk (A.H. Reshak).

0925-8388/$ – see front matter © 2011 Elsevier B.V. All rights reserved.
doi:10.1016/j.jallcom.2011.03.029

cal changes caused due to the addition of Te in CdSe. They studied the effect of various process parameters such as deposition time, temperature, concentration of the basic species, speed of the substrate rotation, pH, etc. on the growth and quality of the films. Azhniuk et al. [6] explored phonon spectra of $CdSe_{1-x}Te_x$ nanocrystals obtained in a borosilicate glass by diffusion-limited process by heat treatment during 2–12 h at temperatures ranging from 625 to 700 °C, resulting in variation of the nanocrystal composition and nanoparticle sizes. Recently Ouendadji et al. [7] have reported a theoretical investigations of the structural, electronic, thermodynamic and optical features of ternary mixed crystals $CdS_{1-x}Se_x$ and $CdS_{1-x}Te_x$ (x = 0.0, 0.25, 0.5, 0.75, 1.0). They have established that the energy band gap is reduced with increasing Te content. Ravichandran et al. [4] experimentally proved that the energy band gap is decreased with increasing Te content for $CdSe_{1-x}Te_x$ (x = 0.2, 0.3, 0.4). Muthukumarasamy et al. [8] have studied the structural phase transformation and optical band gap bowing in hot wall deposited $CdSe_xTe_{1-x}$ (x = 0.0, 0.15, 0.4, 0.6, 0.7, 0.85, 1.0) thin films. Konstantinova-Kabassanova et al. [9] explored the large grain $CdSe_{0.9}Te_{0.1}$ layers grown from the vapor in presence of α-Cr_2O_3. Schenk and Silber [10] have been studied the lattice parameter and microhardness investigations on $CdTe_{1-x}Se_x$. They found that the cubic phase exists in the composition range $0 \le x_{CdSe} \le 0.45$, and the hexagonal phase in the range $0.65 \le x_{CdSe} \le 1.0$.

Although there have been numerous calculations of the electronic structure [11–15], linear optical properties of the parent CdSe and CdTe binary systems have not been intensively studied. As a logical extension to our previous study [16] of the theoretical investigation on the electronic properties, first and second harmonic generation of the CdS, CdSe and CdTe binary systems we thought it would be worthwhile to study the alloys of CdSe and CdTe and investigate the effect of varying Te content in the $CdSe_{1-x}Te_x$ ternary alloys on the band structure and finally on the linear and nonlinear optical susceptibilities using the full potential linear augmented plane wave (FP-LAPW) method [17–19]. This fact may be used in the future for molecular engineering, search and design of the crystals with better SHG by manipulating of the electronic structures with different compositions to achieve more delocalized atomic bonds. To the best of our knowledge, the dispersion of linear and nonlinear optical susceptibilities of these ternary alloys have not been measured or calculated yet. Thus our main goal of this work is to study the effect of increasing concentration of tellurium on the band structure, and as a consequence the spectral dispersion of the linear and nonlinear optical susceptibilities of the cadmium–selenide–telluride alloys $CdSe_{1-x}Te_x$ (x = 0.0,0.25,0.5,0.75 and 1.0) in the cubic structure and (x = 0.0, 0.25) in wurtzite structure. We believe that our study will provide a quantitative theoretical prediction for such properties, and it would be interesting if these are experimentally confirmed.

The most important technical details of our calculations are discussed in Section 2. The core of the article appears in Sections 3 and 4, where the results of electronic properties and the linear and nonlinear optical susceptibilities are presented and analyzed. The article is finished with a short exposition of the main results.

2. Computational details

An all electron full potential linearized augmented plane wave (FPLAPW) method has been used for an *ab initio* theoretical study of the effect of increasing the concentration of tellurium on the band structure, density of states, and the spectral features of the linear and nonlinear optical susceptibilities of the cadmium–selenide–telluride alloys $CdSe_{1-x}Te_x$ (x = 0.0,0.25,0.5,0.75,1.0). In this work, we have used the 'special quasirandom structures' (SQS) approach of Zunger et al. [20] to reproduce the randomness of the alloys for the first few shells around a given site. This approach is reasonably sufficient to describe the alloys with respect to many physical properties that are not affected by the errors introduced using the concept of the periodicity beyond the first few shells.

In this paper, self-consistent calculations using a relativistic FP-LAPW method were carried using the WIEN2K package [19]. For this, a satisfactory degree of convergence was achieved by considering a number of FP-LAPW basis functions up to $R_{MT}K_{max}$ equal to 9 (where R_{MT} is the minimum radius of the muffin-tin spheres and K_{max} gives the magnitude of the largest $\boldsymbol{k}$ vector in the plane wave expansion). In order to keep the same degree of convergence for all the lattice constants studied, we kept the values of the sphere radii and K_{max} constant over all the range of lattice spacing considered. However, Fourier expanded charge density was truncated at G_{max} = 12 (a.u)$^{-1}$. For the cubic structure we have chosen the muffin radii (MT) to be equal to 2.5 a.u for Cd, and 2.4 a.u for Se and Te. For the wurtzite structure of $CdSe_{1-x}Te_x$ (x = 0.0 and 0.25) the MT radii were chosen to be 2.3 and 2.1 a.u for Cd and Se for x = 0.0, and 2.4, 2.3 and 2.5 a.u for Cd, Se, and Te, respectively for x = 0.25. The spherical harmonics inside the muffin-tins were chosen with a cut-off of l_{max} = 6. The exchange and correlation effects were treated by the Perdew–Burke–Ernzerhof generalized gradient approximation GGA-PBE [21]. In addition, for the electronic band structure and optical properties the Engel–Vosko (EV-GGA) scheme [22] was applied. The latter approximation is applied to overcome the shortcoming of the underestimation of the energy gaps in both LDA and GGA [23]. This shortcoming is ascribed to the fact that LDA and GGA do not reproduce the exchange correlation energy and its charge derivative correctly. Therefore EV-GGA is a modified form of GGA, which is able to better reproduce the exchange potential at the expense of less agreement in the exchange energy, which yields a better band splitting. The dependence of the total energy on the number of $\boldsymbol{k}$-points in the irreducible wedge of the first Brillouin zone (BZ) has been explored within the linearized tetrahedron scheme [24] by performing the calculation for 1400 $\boldsymbol{k}$-points within the irreducible Brillouin zone (IBZ). The self-consistency was assumed to be achieved when the total energy difference between successive iterations was less than 10^{-5} Ry per formula unit.

3. Structural properties and phase transitions

Our basic procedure in this work is to calculate the total energy as a function of unit-cell volume around the equilibrium cell volume V_0 for the crystal structures under consideration. Fig. 1 shows the calculated total energies versus volume for the cadmium–selenide–telluride alloys $CdSe_{1-x}Te_x$ (x = 0.0, 0.25, 0.5, and 0.75). The calculated total energies are fitted to an empirical functional form (the third-order Murnaghan's equation of state) [25] to obtain an analytical interpolation of our computed points from which we calculate the structural properties (equation of state, transition pressure, etc.). The cubic structure can be fully described by just the lattice parameter, a. The hexagonal structure (with two formula units per primitive unit cell) can be described by three structural parameters: a, c and an internal parameter, u that determines the relative position of the anion and cation sublattices along the c axis.

In agreement with earlier *ab initio* calculations and with experiment, we have found that following Fig. 1a, there is co-existence of the two phases for CdSe, namely the zinc-blend and wurtzite. The difference of the total energies between the two phases is in the order of 10^{-3} eV. From Fig. 1a, one can see that the stable phase is the wurtzite one. Fig. 1b shows that the most stable phase for $CdSe_{0.75}Te_{0.25}$, is the wurtzite. Whereas for the other structures of $CdSe_{1-x}Te_x$ (x = 0.5 and 0.75) the cubic phase is the

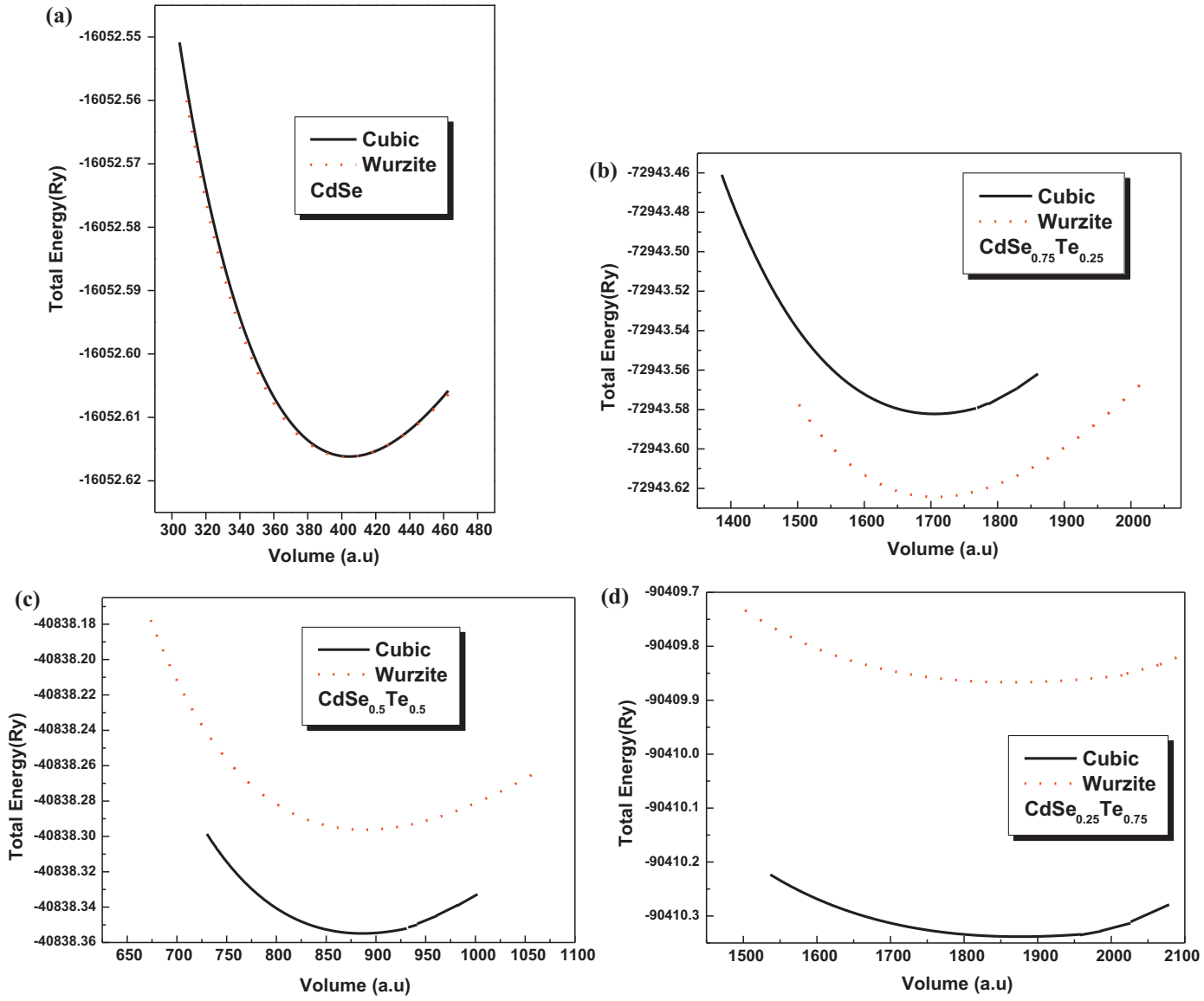

Fig. 1. Variation of total energies versus the volume of unit cell for $CdSe_{1-x}Te_x$ (x = 0.0, 0.25, 0.5, and 0.75), cubic structure (solid curve) and wurtzite structure (dashed curve) calculated using the GGA.

most stable phase (see Fig. 1c and d). Following the experimental work [26] it is found that CdTe crystallizes in the cubic phase at ambient conditions. According to these results one can conclude that within x = 0–0.25 the alloys exist in wurtzite phase and within x = 0.5–1.0, the alloys exist in cubic phase. We expect that a structural phase transition occurs in the range of x varying from 0.0 up to 0.25 in agreement with experimental observation [10]. The calculated structural parameters of the $CdSe_{1-x}Te_x$ (x = 0.0, 0.25, 0.5, 0.75 and 1.0) are listed in Table 1, in comparison with the available experimental data and other theoretical results.

4. Electronic and optical properties

4.1. Band structure and density of states

In this section the band structure and density of states along with the Cd-s/p/d, Se-s/p/d and Te-s/p/d partial density of states of the cadmium–selenide–telluride $CdSe_{1-x}Te_x$ (x = 0.0, 0.25,0.5, 0.75 and 1.0) are reported. Fig. 2 shows the band structure of the alloys for various Te content. For the cubic structure with the increasing Te content the band gap is decreased in agreement with the previous calculations using the same approach [7] and the experimental results for x = 0.2, 0.3, 0.4 [4]. Increasing Te content leads to a shift of the conduction band (CB) towards the Fermi energy (E_F) resulting in decrease of the energy band gap. The band gaps are 0.95 (1.76), 0.89 (1.65), 0.83 (1.56), 0.79 (1.44) and 0.76 (1.31) eV within a framework of GGA (EV-GGA) approach for x = 0.0, 0.25, 0.5, 0.75 and 1.0. The valence band maximum (VBM) remains fixed. The conduction band minimum (CBM) and the valence band maximum (VBM) are located at the centre of the BZ (Γ point) confirming a direct gap feature. Since the wurtzite phase is the stable phase for both of CdSe and $CdSe_{0.75}Te_{0.25}$ we show the band structure and the total DOS a long with the partial DOS for this phase. We find that the wurtzite structure maintain the direct gap feature with energy band gap values equal to about 0.8 (1.6) eV for x = 0.0 and about 0.7 (1.55) eV for x = 0.25, within a framework of GGA (EV-GGA) approach.

Previous studies [27,28] have shown that the use of the LDA and GGA usually leads to underestimate the energy band gaps in semiconductors. Moreover, both of LDA and GGA functional are based on simple model assumptions which are not sufficiently flexible for accurate reproduction of the exchange correlation energy and its charge space derivative. Engel and Vosko considered this short-

Table 1
Calculated lattice constants and bulk modulus in comparison with the available theoretical and experimental data.

Compounds	a (Å)	c (Å)	a (Å) exp.	c (Å) exp.	B (GPa)	B (GPa) Exp.
CdSe_cubic	6.207* 6.210[d], 6.050[e], 6.216[f],	–	6.084[a,b], 6.050[c]	–	45.600*, 65.12[j] 45.16[l]	53[i]
CdSe_wurzite	4.34*,	7.27*,	4.30[g], 4.30[m]	7.02[g], 7.01[m]	43.635*	
$CdSe_{0.75}Te_{0.25}$_cubic	6.526*	–			43.079*	
$CdSe_{0.75}Te_{0.25}$_wurzite	4.429*	14.891*			42.318*	
$CdSe_{0.5}Te_{0.5}$_cubic	6.407*	–			42.206*	
$CdSe_{0.5}Te_{0.5}$_wurzite	4.437*	7.459*			39.135*	
$CdSe_{0.25}Te_{0.75}$_cubic	6.322*	–			40.138*	
$CdSe_{0.25}Te_{0.75}$_wurzite	4.563*	14.653*			36.311*	
CdTe_cubic	6.620*, 6.626[d], 6.48[e], 6.631[f], 6.54[h]	–	6.48[a,c], 6.54[b], 6.477[h]	–	36.242*, 44.5[k], 48.94[j], 33.78[l]	44.5[i]
CdTe_wurzite	4.68*, 4.56[h]	7.65* 7.54[h]	4.57[h]	7.47[h]	34.621*	

[a] Ref. [26].
[b] Ref. [64].
[c] Ref. [59].
[d] Ref. [60].
[e] Ref. [61].
[f] Ref. [7].
[g] Ref. [37].
[h] Ref. [66].
[i] Ref. [59].
[j] Ref. [61].
[k] Ref. [62].
[l] Ref. [7].
[m] Ref. [10].
* This work.

coming and constructed a new functional form of GGA which is able to reproduce better the exchange potential at the expense of less agreement in the exchange energy. This approach called EV-GGA [22] yields better band splitting and some other properties which are crucially dependent on the accuracy of exchange correlation potential. Therefore, we have selected the EV-GGA approach to determine the electronic band structure and spectral linear and nonlinear optical properties.

The total density of states (TDOS) and partial density of states (PDOS) are shown in Figs. 3 and 4. The band structure and density of states of the investigated binary and ternary alloys can be divided into five principal groups/structures. We have analyzed the contribution of the anion and cation's originated band states to each set of bands by decomposing the total density of states into s-, p-, and d-orbital contributions. Following the PDOS we are able to identify the angular momentum characters of various structures; the structure ranging from −13.0 to −10.0 eV is mainly originating from Cd-s/p, Se-s and Te-s states. From Fig. 3a, g and m, one can emphasize that increasing Te content from 0.25 to 0.5 to 0.75 leads to the reduction of the TDOS and drastically increases the second spectral peak situated around −10.0 eV. Fig. 4a and d, show that the wurtzite structure confirms the same behavior. The energy region from −8.4 eV to −7.0 eV is prevailingly formed by Cd-d states with an admixture of Te-s/p. The DOS energy region from −4.0 eV up to Fermi energy is originated from Se/Te-s/p, Cd-s/p states with a small admixture of Se/Te-d. The conduction bands are composed prevailingly of Se/Te-p/d and Cd-s/p states. The Cd-p states are reduced with increasing concentration of Te, while there is a small increase in the Cd-s states (see Fig. 3b, f and j). The $CdSe_{0.75}Te_{0.25}$ alloy contains three Se atoms and one Te atom. When we replace one of Se atoms by Te atom to form the $CdSe_{0.5}Te_{0.5}$ alloy we notice that the amplitude of Se-s/p and Te-s/p structures increases whereas when we replaced one of Se atoms from the $CdSe_{0.5}Te_{0.5}$ alloy by one Te atom to form the $CdSe_{0.25}Te_{0.75}$ alloy we observe that the amplitude of the Se-s/p structures are substantially increased while the amplitudes of Te-s/p atoms are significantly reduced. From the partial density of states one can see that there exists a strong hybridization between Se-s and Se-p in the energy region between 6.0 and 11.0 eV. At the energy regions between 6.0 and 7.0 eV and 8.0 and 11.0 eV Te-s states are strongly hybridized with Te-p, Se-s/p and Te-s/p states. At the low energy ranges between −13.0 and −5.0 eV we have found that Cd-s is hybridized with Cd-p.

We can elucidate the nature of chemical bonding from the total and partial DOS spectra. We observe that the DOS, extending from −13.0 eV to Fermi energy (E_F) is larger for Cd-d states (20.0 electrons/eV), Cd-s states (1.0 electrons/eV), Se-s states (14 electrons/eV), Te-s states (4.0 electrons/eV), Se-p (2.0 electrons/eV), and Te-p (1.2 electrons/eV) with respect to the total DOS with the angular momentum projected DOS of Cd-s/d and Te/Se-s/p states as shown in Fig. 3. These results also show that some electrons from Cd-s/d and Te/Se-s/p states are transferred into valence bands (VBs) and contribute in weak covalence interactions between Cd–Cd, Se–Se and Te–Te atoms, and the substantial covalence interactions between Cd and Se, Cd and Te, and Se–Te atoms. All the Cd–Cd, Se–Se and Te–Te bonds are mainly of covalent character, and Cd–Se Cd–Te, and Se–Te bonds are of ionic character. Accordingly, we can also say that the covalent strength of Cd–Se, Cd–Te, and Se–Te bonds are weaker than that of Cd–Cd, Se–Se and Te–Te bonds.

4.2. Linear optical susceptibilities

As it has mentioned above that both LDA and GGA lead to underestimate the energy band gaps in semiconductors and since the energy band differences enter the calculations of response functions in the denominators of the expressions they will play a major rule in the values of the susceptibilities, so it is not surprising that the latter values will be overestimated. That will lead to errors of the order of 10–30% in linear response. The problem is aggravated in higher-order responses by the fact that denominators occur in higher powers [29]. In order to overcome this shortcoming we have used the EV-GGA approach. The linear response of the system to electromagnetic radiation can be described by means of the dielectric function $\varepsilon(\omega)$ which is related to the interaction of photons with electrons. Two kinds of contributions to $\varepsilon(\omega)$ are usually distinguished, namely intra-band and inter-band electronic excitations. Intra-band transitions are not present in semiconductors, as they are present only for metals and semi-metals. The dispersion of the imaginary part of the dielectric function $\varepsilon_2(\omega)$ can be calculated from the momentum matrix elements between the occupied and unoccupied wave-functions, giving rise to the selection rules. The

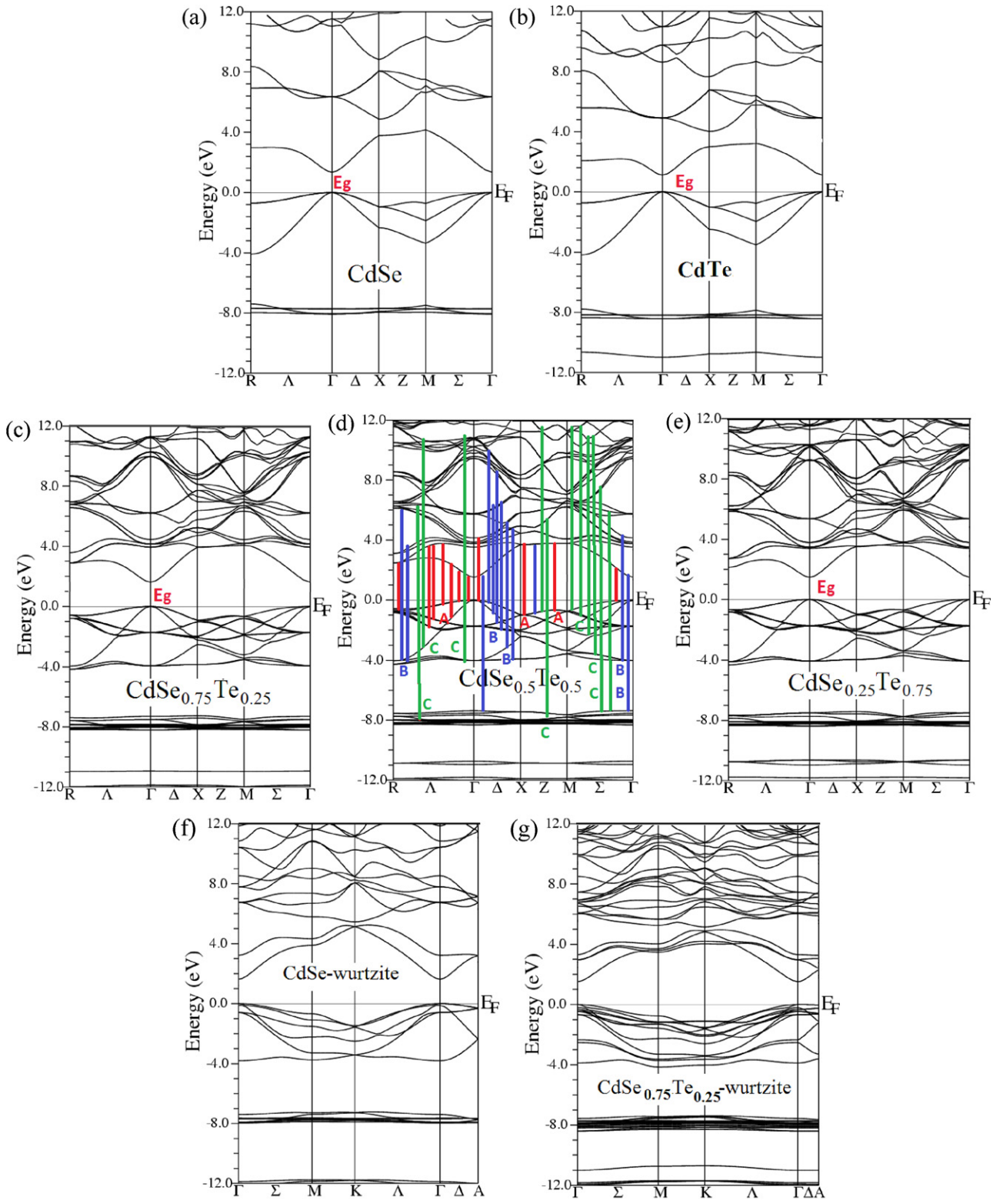

Fig. 2. The calculated band structure along with the optical transitions depicted on a generic band structure of the cubic cadmium selenide telluride binary and ternary alloys $CdSe_{1-x}Te_x$ (x = 0.0, 0.25,0.5,0.75 and 1.0) and wurtzite $CdSe_{1-x}Te_x$ (x = 0.0, 0.25).

real part $\varepsilon_1(\omega)$ of the dielectric function can be evaluated from the imaginary part $\varepsilon_2(\omega)$ by the Kramer–Kronig relationship [30]. All the other optical constants can be derived from $\varepsilon_1(\omega)$ and $\varepsilon_2(\omega)$. To calculate the optical spectra of the dielectric function, $\varepsilon(\omega)$, a dense mesh of uniformly distributed ***k***-points is required. Hence, the Brillouin zone integration was performed with 1400 ***k***-points in the irreducible part of the Brillouin zone for both linear and nonlinear optical properties, with broadening equal to 0.1 eV to

bring out all the structures. This value is typical of the experimental accuracy.

Figs. 5a and b and 6a, b, d and e, display the imaginary and real parts of the electronic dielectric function $\varepsilon(\omega)$ spectra for a spectral energies up to 14.0 eV for the cubic structure of $CdSe_{1-x}Te_x$ (x = 0.0, 0.25,0.5, 0.75 and 1.0) and the wurtzite structure of $CdSe_{1-x}Te_x$ (x = 0.0, 0.25). The analysis of $\varepsilon_2(\omega)$ curve shows that the threshold energy (first critical point) of the dielectric function occurs at 1.76, 1.65, 1.56, 1.44, and 1.31 eV for the cubic CdSe, $CdSe_{0.75}Te_{0.25}$, $CdSe_{0.5}Te_{0.5}$, $CdSe_{0.25}Te_{0.75}$ and CdTe, respectively. For the wurtzite structures of CdSe and $CdSe_{0.75}Te_{0.25}$ the threshold energy of $\varepsilon_2^{II}(\omega)$ and $\varepsilon_2^{\perp}(\omega)$ is around 1.74, 1.6 eV, respectively. This point is the $(\Gamma_v$–$\Gamma_c)$ splitting, which gives the threshold for direct optical transitions between the VBM and the CBM. This is known as the fundamental absorption edge. The origin of these peaks is attributed to the inter-band transitions form the occupied Cd-s/p/d and Se/Te-s/p/d band states to the unoccupied Cd-s/p and Se/Te-s/p/d band states. Beyond these threshold energies (first critical points), the curve increases rapidly. This is due to the fact that the number of points contributing towards $\varepsilon_2(\omega)$ is increased abruptly. The main peak of $\varepsilon_2(\omega)$ for the cubic CdSe, $CdSe_{0.75}Te_{0.25}$, $CdSe_{0.5}Te_{0.5}$, $CdSe_{0.25}Te_{0.75}$ and CdTe, binary and ternary alloys is situated between two humps. The main peaks are located at around 6.5,

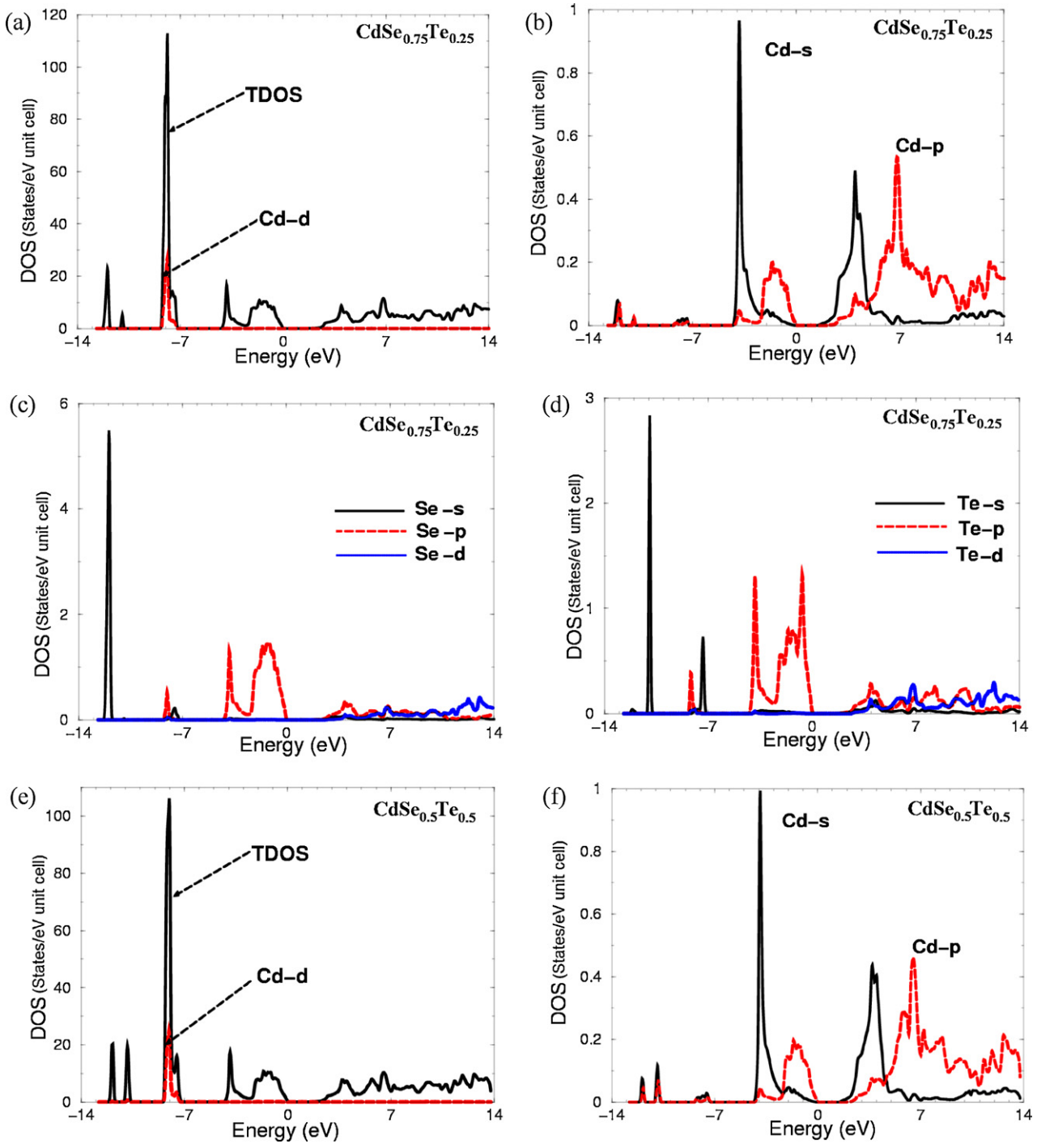

Fig. 3. Calculated total and partial densities of states (states/eV unit cell) of the cubic cadmium selenide telluride ternary alloys $CdSe_{1-x}Te_x$ (x = 0.25, 0.5 and 0.75) and wurtzite $CdSe_{1-x}Te_x$ (x = 0.0, 0.25).

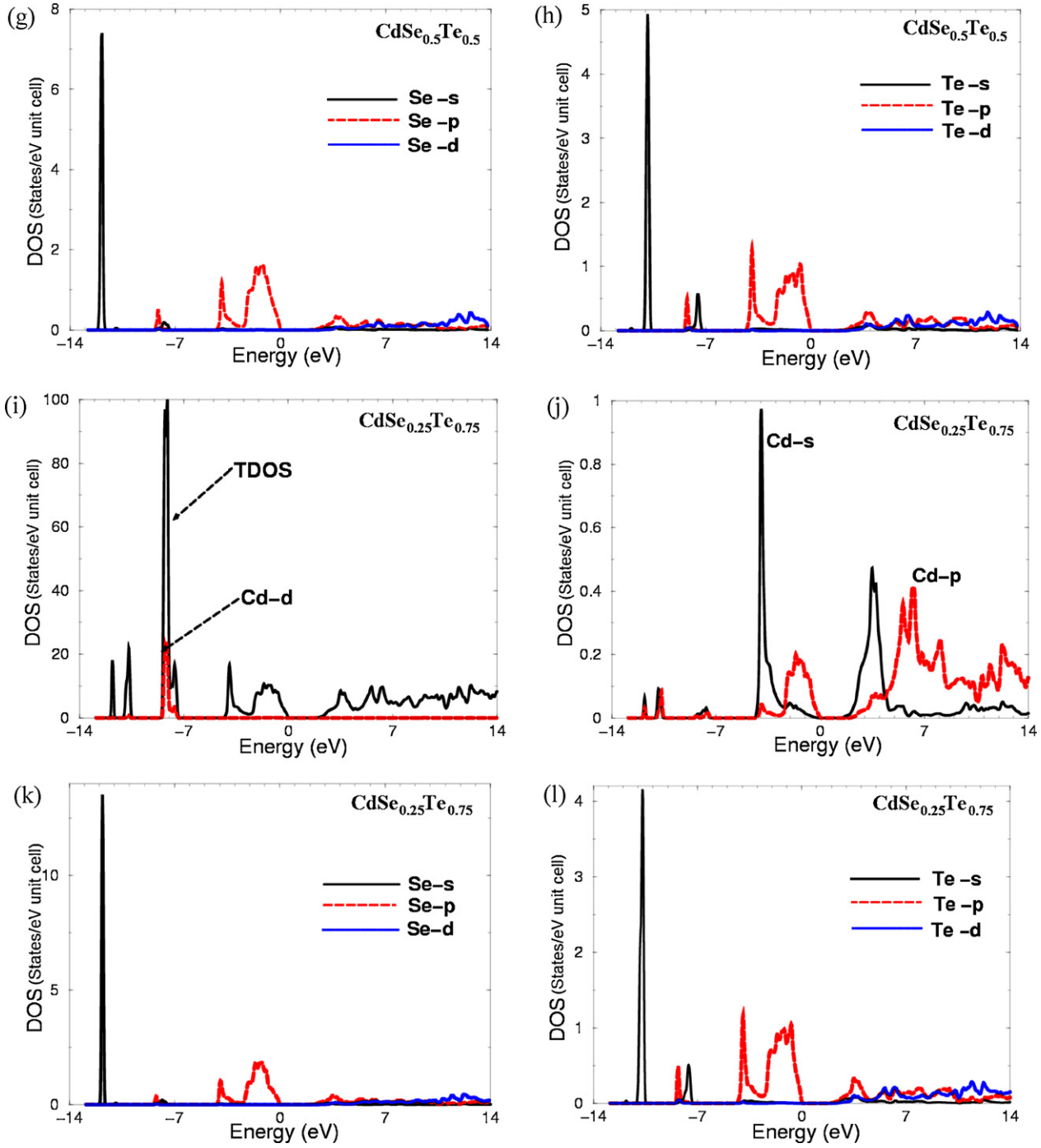

Fig. 3. (*Continued*)

5.7, 5.6, 5.2, and 4.9 eV for CdSe, $CdSe_{0.75}Te_{0.25}$, $CdSe_{0.5}Te_{0.5}$, $CdSe_{0.25}Te_{0.75}$ and CdTe, respectively. Following Fig. 5a one can see that the structures of $\varepsilon_2(\omega)$ for all the alloys are spectrally shifted towards lower energies with increasing the amplitude when the concentration of Te increases, which confirms our previous observation that the energy band gap is reduced with increasing the concentration of Te. The wurtzite structure of CdSe and $CdSe_{0.75}Te_{0.25}$ shows two principal peaks for both of $\varepsilon_2^{\perp}(\omega)$ and $\varepsilon_2^{\mathrm{II}}(\omega)$. These two main peaks are located at around 5.0 and 7.5 eV for CdSe and 4.5 and 7.0 for $CdSe_{0.75}Te_{0.25}$ for $\varepsilon_2^{\perp}(\omega)$ and $\varepsilon_2^{\mathrm{II}}(\omega)$, respectively which confirms our previous observation that the energy band gap is reduced with increasing the concentration of Te.

In order to identify the spectral peaks in the linear optical spectra we considered the optical transition matrix elements. We used our calculated band structure to indicate the transitions, indicating the major structure for the principal components $\varepsilon_2(\omega)$ in the band structure diagram. These transitions are labeled according to the spectral peak positions in Fig. 5a. For simplicity we have labeled the transitions in Figs. 2 and 5a, as *A*, *B*, and *C*. The transitions (*A*) are responsible for the structures for $\varepsilon_2(\omega)$ in the spectral range 0.0–5.0 eV; the transitions (*B*) 5.0–10.0 eV, and the transitions (*C*) 10.0–14.0 eV. As prototype we show these transitions only for $CdSe_{0.5}Te_{0.5}$. The estimated values of the static optical dielectric constant $\varepsilon_1(0)$, which is also called higher frequency dielectric constant because it does not include the phonon effect, are listed

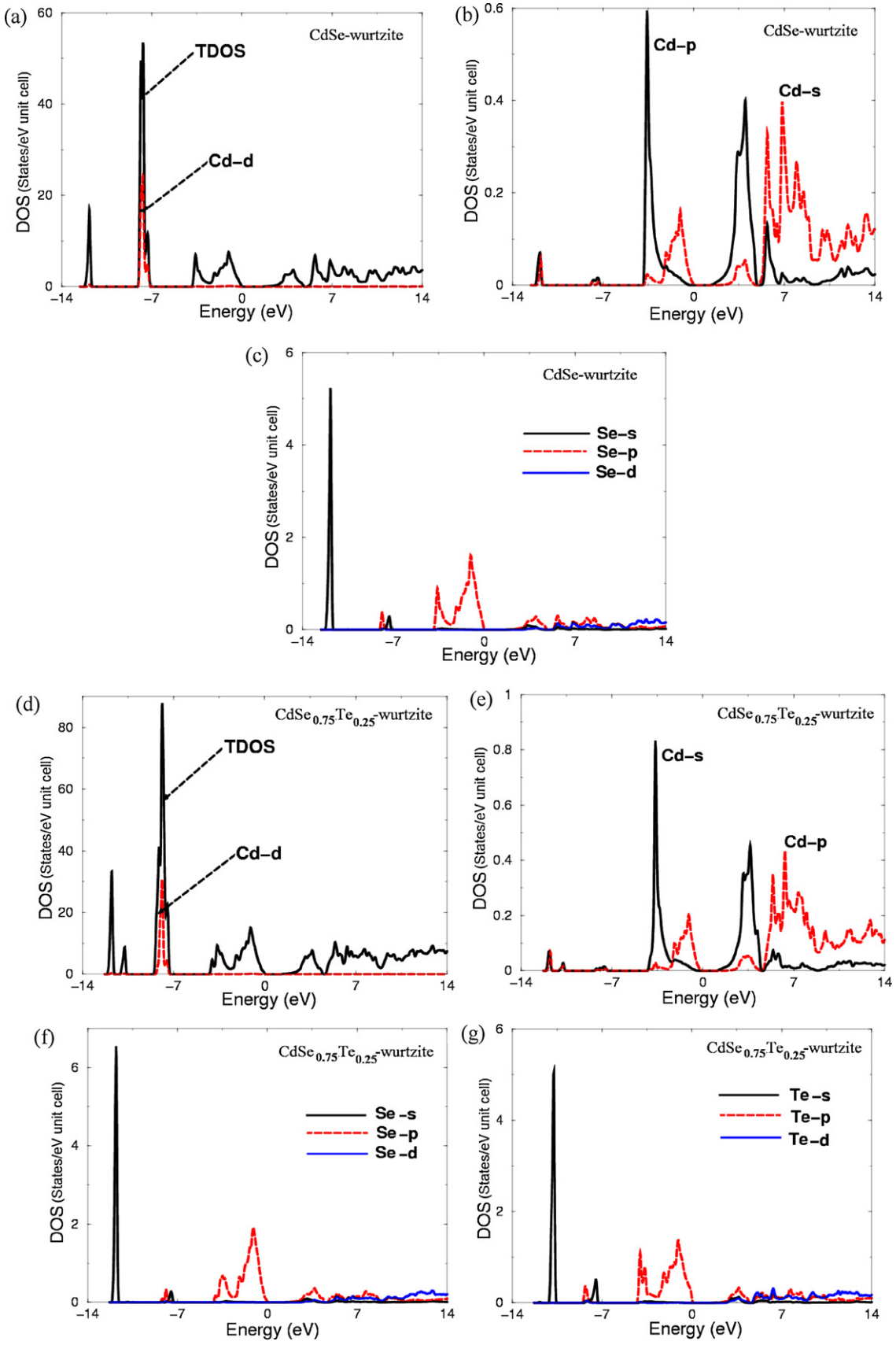

Fig. 4. Calculated total and partial densities of states (states/eV unit cell) of the wurtzite $CdSe_{1-x}Te_x$ ($x = 0.0, 0.25$).

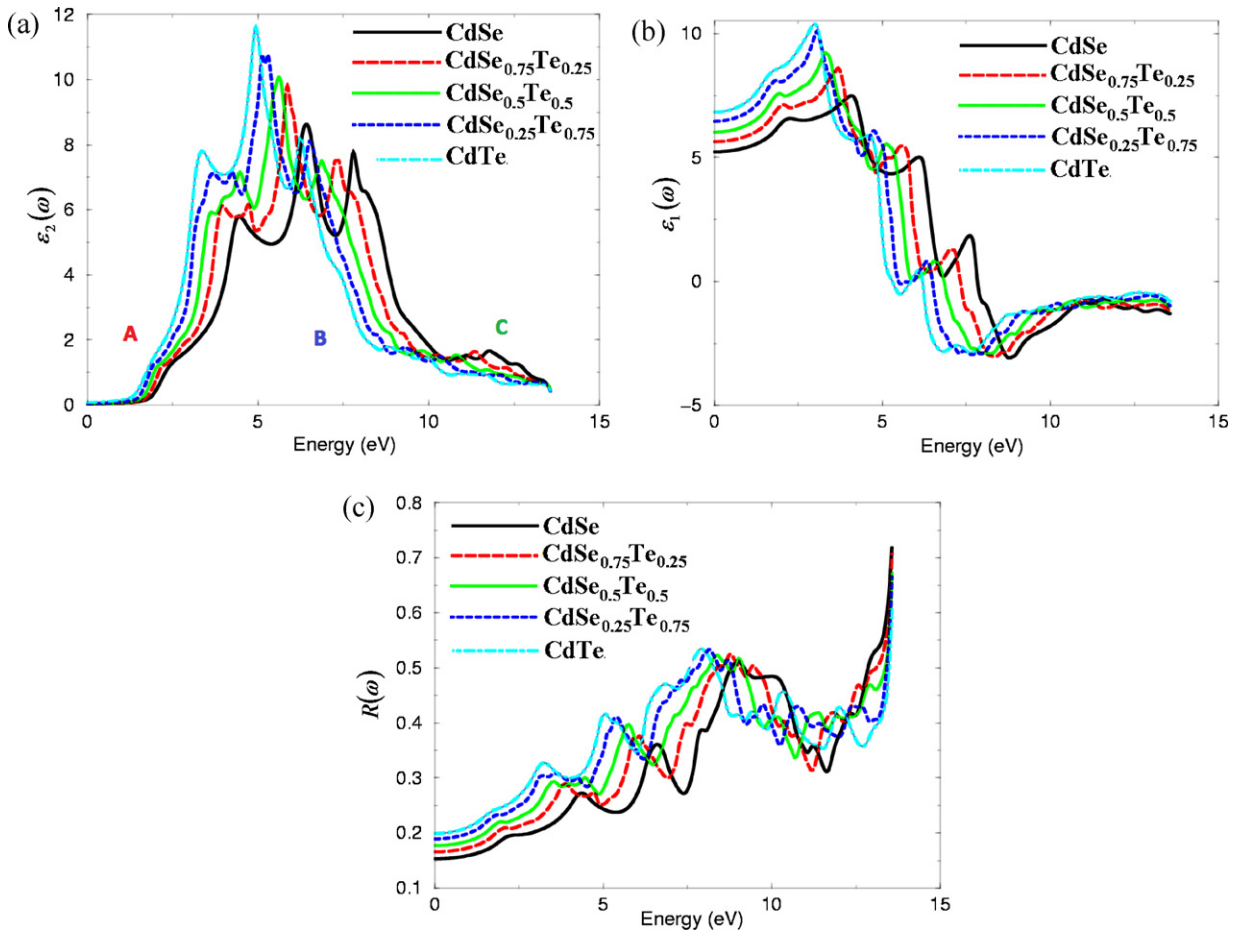

Fig. 5. (a) Calculated $\varepsilon_2(\omega)$ spectra. (b) Calculated $\varepsilon_1(\omega)$ spectra. (c) Calculated total $R(\omega)$. For the cubic cadmium selenide telluride binary and ternary alloys $CdSe_{1-x}Te_x$ (x = 0.0, 0.25, 0.5, 0.75 and 1.0).

Table 2
Calculated energy gaps, static dielectric constants $\varepsilon_1(0)$, $\varepsilon_1^{\perp}(0)$ and $\varepsilon_1^{\text{II}}(0)$, in comparison with the available theoretical and experimental data.

Compounds	CdSe	$CdSe_{0.75}Te_{0.25}$	$CdSe_{0.5}Te_{0.5}$	$CdSe_{0.25}Te_{0.75}$	CdTe
E_g (GGA)	0.95*, 0.8**	0.89*, 0.7**	0.83*	0.79*	0.76*
E_g (EV-GGA)	1.76*, 1.6**	1.65*, 1.55**	1.56*	1.44*	1.31*
E_g (expt)	1.82[a], 1.84[b], 1.25[c], 1.9[d]	1.425[e]	1.48[f]		1.6[a,d,f], 1.4[b], 1.34[c], 1.83[g]
E_g (theor.)	1.48[a], 2.0[h,i], 1.9[j], 0.95[k], 0.48[l], 1.08[m], 1.2[n]	1.425[e]	0.79[f]		1.24[a], 0.76[k], 0.62[l], 1.88[m], 1.087[n]
$\varepsilon_1(0)$ theor.	5.4*, 5.68[a], 8.5[k]	5.7*	6.0*	6.4*	6.6*, 9.02[a], 9.3[k]
$\varepsilon_1(0)$ expt.	5.8[o]				7.2[p], 8.5[q]
$\varepsilon_1^{\perp}(0)$	5.2**				5.54**
$\varepsilon_1(0)$	5.3**				5.7**

[a] Ref. [26].
[b] Ref. [38].
[c] Ref. [39].
[d] Ref. [59].
[e] Ref. [63].
[f] Ref. [65].
[g] Ref. [66].
[h] Ref. [40].
[i] Ref. [41].
[j] Ref. [42].
[k] Ref. [16].
[l] Ref. [60].
[m] Ref. [61].
[n] Ref. [7].
[o] Ref. [44].
[p] Ref. [45].
[q] Ref. [43].
* This work-cubic.
** This work-wurtzite.

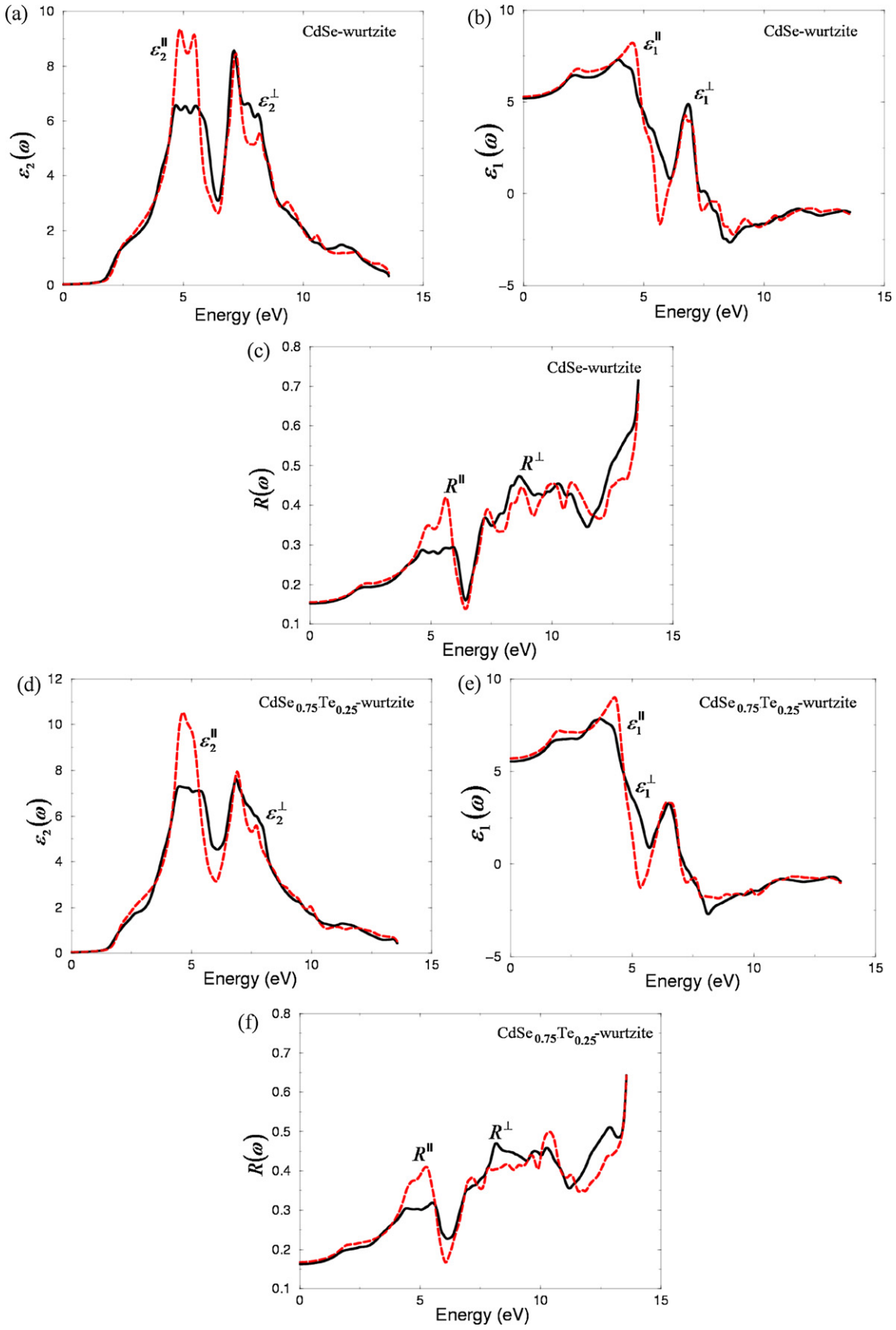

Fig. 6. (a) Calculated $\varepsilon_2^{\perp}(\omega)$ and $\varepsilon_2^{II}(\omega)$ spectra. (b) Calculated $\varepsilon_1^{\perp}(\omega)$ and $\varepsilon_1^{II}(\omega)$ spectra. (c) Calculated total $R(\omega)$. For the wurtzite $CdSe_{1-x}Te_x$ ($x = 0.0, 0.25$).

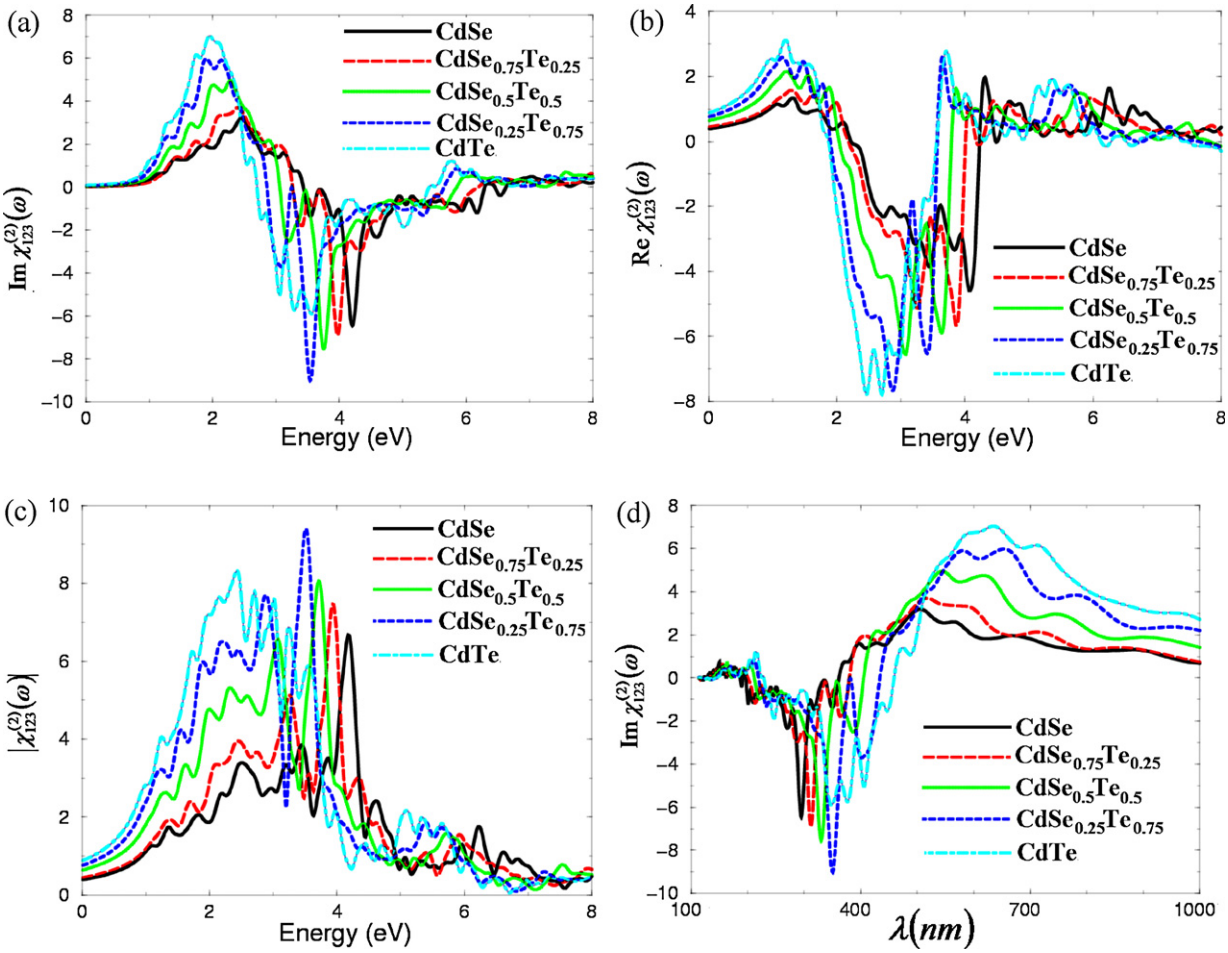

Fig. 7. (a) Calculated $Im\ \chi^{(2)}_{123}(\omega)$ spectra. (b) Calculated $Re\ \chi^{(2)}_{123}(\omega)$. (c) Calculated $\left|\chi^{(2)}_{123}(\omega)\right|$. (d) Calculated nonlinear spectroscopy. For the cubic cadmium selenium telluride binary and ternary alloys $CdSe_{1-x}Te_x$ (x = 0.0, 0.25,0.5,0.75 and 1.0). All the $\chi^{(2)}_{ijk}(\omega)$ and $\left|\chi^{(2)}_{ijk}(\omega)\right|$ are multiplied by 10^{-7}, in esu units.

in Table 2, in comparison with the available experimental and theoretical values. We note that a smaller energy gap yields a larger $\varepsilon_1(0)$ value. This could be explained on the basis of the Penn model [31].

The reflectivity spectra $R(\omega)$ for the binary and ternary alloys CdSe, $CdSe_{0.75}Te_{0.25}$, $CdSe_{0.5}Te_{0.5}$, $CdSe_{0.25}Te_{0.75}$ and CdTe, are shown in Figs. 5c and 6c and f. We should emphasize that the reflectivity minimum which is situated between 10.7 and 11.7 eV for x = 0.0, 0.25, 0.5, 0.75 and 1.0 alloys confirms the occurrence of a collective plasmon resonance. The depth of the plasmon minimum is determined by the imaginary part of the dielectric function at the plasma resonance and is representative of the degree of overlap between the inter-band absorption regions.

4.3. Second harmonic generation

Since $CdSe_{1-x}Te_x$ alloys have cubic structure, hence, $\chi^{(2)}_{123}(-2\omega;\omega;\omega)$ is the only nonzero component, while for the wurtzite structure $\chi^{(2)}_{113}(-2\omega;\omega;\omega)$, $\chi^{(2)}_{311}(-2\omega;\omega;\omega)$ and $\chi^{(2)}_{333}(-2\omega;\omega;\omega)$ are the nonzero components. Both $\chi^{(2)}_{113}(-2\omega;\omega;\omega)$ and $\chi^{(2)}_{311}(-2\omega;\omega;\omega)$ are very small and $\chi^{(2)}_{333}(-2\omega;\omega;\omega)$ is the dominant component. In this work we show only the dominant component. The complex second-order nonlinear optical susceptibility tensor $\chi^{(2)}_{123}(-2\omega;\omega;\omega)$ has been calculated using the expressions given in Refs. [32–34]. The formalisms for calculating the second order susceptibility $\chi^{(2)}_{123}(-2\omega;\omega;\omega)$ for non-magnetic semiconductors and insulators based on the FP-LAPW method have been presented before [33,34]. In the first order responses (linear responses) functions, only the inter-band terms appear and involve only the square of matrix elements, which ensures, for example that $\varepsilon_2(\omega)$ is positive. The second harmonic response involves 2ω resonance in addition to the ω resonance. Both ω and 2ω resonances can be additionally divided into inter-band $\chi^{(2)}_{inter}(-2\omega;\omega;\omega)$, intra-band $\chi^{(2)}_{intra}(-2\omega;\omega;\omega)$ contributions and the modulation on inter-band terms by intra-band terms $\chi^{(2)}_{mod}(-2\omega;\omega;\omega)$ [32–35]. The dipole matrix element values are much stronger in nonlinear case. The real and imaginary parts of the products of matrix elements that determine the strength of a given resonance in $\chi^{(2)}_{123}(-2\omega;\omega;\omega)$ can be positive or negative. The imaginary part of the $\chi^{(2)}_{123}(-2\omega;\omega;\omega)$ for binary and ternary CdSe, $CdSe_{0.75}Te_{0.25}$, $CdSe_{0.5}Te_{0.5}$, $CdSe_{0.25}Te_{0.75}$ and CdTe, $CdSe_{0.25}Te_{0.75}$ alloys is shown in Fig. 7a. We should emphasize that for the concentrations (x = 0.0, 0.25, 0.5, 0.75 and 1.0) increasing the content of Te leads to increase the amplitude and shift all the structures of $\chi^{(2)}_{123}(-2\omega;\omega;\omega)$ towards lower energies that is indicated that increasing the concentration of Te leads to increase the value of the second harmonic generation. Fig. 8a shows the imaginary part of the dominant component $\chi^{(2)}_{333}(-2\omega;\omega;\omega)$ for wurtzite structure of CdSe and $CdSe_{0.75}Te_{0.25}$. It is clear that the wurtzite structure shows different structure than the cubic one for the same compound.

Table 3
Calculated $||\chi^{(2)}_{123}(0)|$, $|\chi^{(2)}_{333}(0)|$, (pm/V), $|\chi^{(2)}_{123}(-2\omega;\omega;\omega)|$ and $|\chi^{(2)}_{333}(-2\omega;\omega;\omega)|$ (pm/V) at 1064 nm, in comparison with the available theoretical and experimental data.

Compounds	CdSe	$CdSe_{0.75}Te_{0.25}$	$CdSe_{0.5}Te_{0.5}$	$CdSe_{0.25}Te_{0.75}$	CdTe
$\|\chi^{(2)}_{123}(0)\|$ pm/V	16.75[a*]	18.85[a*]	27.23[a*]	32.25[a*]	37.70[a*]
$\|\chi^{(2)}_{333}(0)\|$ pm/V	12.65[a**]	21.11[a**]			
$\|\chi^{(2)}_{123}(-2\omega;\omega;\omega)\|$ at 1064 nm (pm/V)	54.46[a*]	64.51[a*]	98.44[a*]	134.05[a*]	147.04[a*]
$\|\chi^{(2)}_{333}(-2\omega;\omega;\omega)\|$ at 1064 nm (pm/V)	25.13[a**]	49.43[a**]			
$\chi^{(2)}_{123}(0)$ expt. (1×10^{-8} esu)	54[b], 26[c], 14.8[c], 26[d], 13.6[c]				80[c], 28.2[e]
$\chi^{(2)}_{123}(0)$ theor. (1×10^{-8} esu)	20[g], 25[f]				27[h], 134[i], 71[j], 60[k], 132[l], 33[m], 35[g], 84[n], 24.8[o], 80[f]

[a*] This work-cubic.
[a**] This work-wurtzite.
[b] Ref. [46].
[c] Ref. [47].
[d] Ref. [48].
[e] Ref. [49].
[f] Ref. [16].
[g] Ref. [50].
[h] Ref. [51].
[i] Ref. [52].
[j] Ref. [53].
[k] Ref. [54].
[l] Ref. [55].
[m] Ref. [56].
[n] Ref. [57].
[o] Ref. [58].

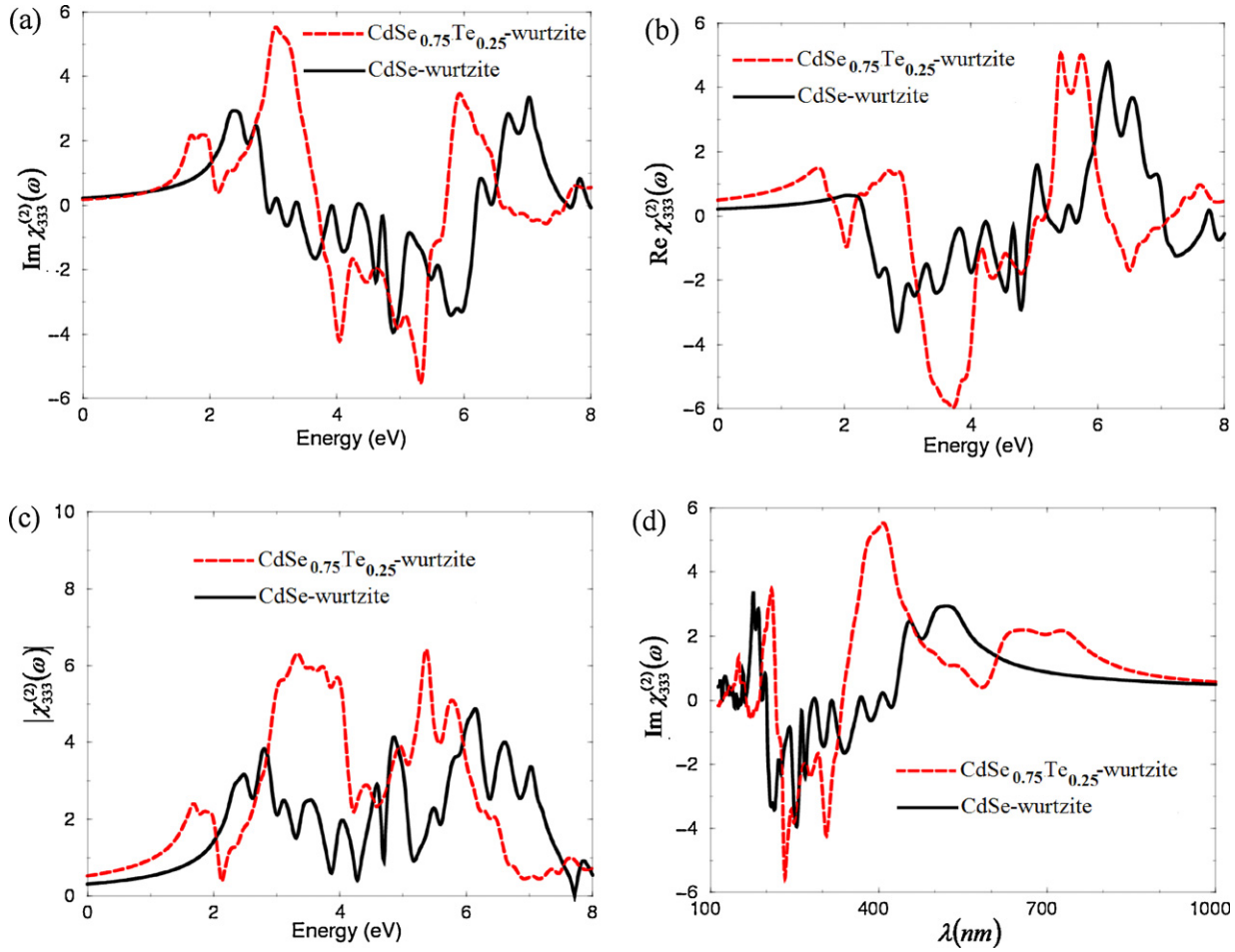

Fig. 8. (a) Calculated $Im\chi^{(2)}_{333}(\omega)$ spectra. (b) Calculated $Re\chi^{(2)}_{333}(\omega)$. (c) Calculated $\left|\chi^{(2)}_{333}(\omega)\right|$. (d) Calculated nonlinear spectroscopy. For the wurtzite cadmium selenium telluride binary and ternary alloys $CdSe_{1-x}Te_x$ (x = 0.0, 0.25). All the $\chi^{(2)}_{ijk}(\omega)$ and $\left|\chi^{(2)}_{ijk}(\omega)\right|$ are multiplied by 10^{-7}, in esu units.

Looking at Figs. 7b and 8b one can see that the values of Re $\chi^{(2)}_{123}(0)$ are increasing when we increase the content of Te for both of the cubic and wurtzite structure (see Table 3). That is attributed to the fact that the nonlinear optical properties are more sensitive to small changes in the band structure than the linear optical properties due to higher power energy difference in the denominators of the formalism [given in Refs. [33,34]]. Moreover, in the static limit, the SHG coefficients show the general trend of having an inverse correlation with the band gaps [36]. In general, smaller band gaps yield larger $\chi^{(2)}_{ijk}(-2\omega;\omega;\omega)$ values due to smaller energy differences in the denominator of the formalism [given in Refs. [33,34]], but only if the electronic structures are not significantly changed. The second harmonic response involves 2ω resonance terms in addition to the usual ω resonance and the threshold for 2ω parts occurs at the half energy of the threshold for ω part, as a result, only the 2ω inter/intra terms contributes to $\chi^{(2)}_{123}(-2\omega;\omega;\omega)$ in the energy range below the fundamental energy band gap. Figs. 7c and 8c displays our calculated $|\chi^{(2)}_{123}(-2\omega;\omega;\omega)|$ and $|\chi^{(2)}_{333}(-2\omega;\omega;\omega)|$. Again it shows that with increasing Te content all the spectral structures of $|\chi^{(2)}_{123}(-2\omega;\omega;\omega)|$ and $|\chi^{(2)}_{333}(-2\omega;\omega;\omega)|$ are shifted towards lower energies with increasing the values of $|\chi^{(2)}_{123}(0)|$ and $|\chi^{(2)}_{333}(0)|$ as a function of the tellurium concentration. These values and $|\chi^{(2)}_{123}(-2\omega;\omega;\omega)|$ and $|\chi^{(2)}_{333}(-2\omega;\omega;\omega)|$ at $\lambda = 1064$ nm are given in Table 3, along with the available experimental and theoretical values. From Figs. 7d and 8d, showing the nonlinear spectroscopy of these alloys, it is clear that these alloys show considerable nonlinear optical spectra in the wavelength starting from vacuum ultraviolet spectral range up to infrared that makes these alloys to be applicable in this wide spectral range.

5. Conclusion

In this work we have performed first principle calculations of the electronic band structures, density of states, and the linear and nonlinear optical susceptibilities for the $CdSe_{1-x}Te_x$ alloys within a framework of FP-LAPW method. The analysis of our calculations confirms the enhancement of the nonlinear optical functionality of the $CdSe_{1-x}Te_x$ alloys with increasing the concentration of Te. Calculations are reported for the spectral features of the linear and nonlinear optical susceptibilities. We can emphasize that increasing Te content leads to significant enhancement of the effective second-order susceptibility coefficients from 16.75 pm/V (CdSe) to 18.85 ($CdSe_{0.75}Te_{0.25}$), 27.23 ($CdSe_{0.5}Te_{0.5}$), 32.25 ($CdSe_{0.25}Te_{0.75}$), and 37.70 (CdTe) pm/V. To the best of our knowledge, the linear and nonlinear optical features of these alloys have not been measured or calculated yet. Hence, our study may serve as a quantitative theoretical prediction for such properties. This work may be used in the future for engineering, search and design of the crystals with better SHG by manipulating of the electronic structures of these materials with different compositions to achieve more delocalized atomic bonds.

Acknowledgements

This work was supported from the institutional research concept of the Institute of Physical Biology, UFB (No.MSM6007665808), the program RDI of the Czech Republic, the project CENAKVA (No. CZ.1.05/2.1.00/01.0024), the grant No. 152/2010/Z of the Grant Agency of the University of South Bohemia. School of Material Engineering, Malaysia University of Perlis, P.O Box 77, d/a Pejabat Pos Besar, 01007 Kangar, Perlis, Malaysia. The author Rabah Khenata extends his appreciation to the Deanship of Scientific Research at King Saud University for funding the work through the research group project No RGP-VPP-088.

References

[1] W. Lotz, J. Opt. Soc. Am. 60 (1970) 206.
[2] R.E. Bailey, J.B. Strausburg, S. Nie, J. Nanosci. Nanotechnol. 4 (2004) 569–574.
[3] V.D. Das, Proc. SPIE 1523 (1992) 326–333, Conf on Physics and Technology of Semiconductor Devices and Integrated Circuits.
[4] D. Ravichandran, F.P. Xavier, S. Sasikala, S.M. Babu, Bull. Mater. Sci. 19 (1996) 437–442.
[5] P.D. More, G.S. Shahane, L.P. Deshmukh, P.N. Bhosale, Mater. Chem. Phys. 80 (2003) 48–54.
[6] Y. Azhniuk, Y.I. Hutych, V.V. Lopushansky, L.A. Prots, A.V. Gomonnai, D.R.T. Zahn, Phys. Status Solidi (c) 6 (9) (2009) 2064–2067.
[7] S. Ouendadji, S. Ghemid, H. Meradji, F.El. Haj Hassan, Comput. Mater. Sci. 48 (2010) 206–211.
[8] N. Muthukumarasamy, S. Jayakumar, M.D. Kannan, R. Balasundaraprabhu, Solar Energy 83 (2009) 522–526.
[9] E. Konstantinova-Kabassanova, Z. Nenova, A. Lusson, Y. Marfaing, K. Kabassanov, Y. Bistrev, J. Mater. Sci.: Mater. Electron. 11 (2000) 679–683.
[10] M. Schenk, C. Silber, J. Mater. Sci.: Mater. Electron. 9 (1998) 295–300.
[11] D.J. Chadi, J.P. Walter, M.L. Cohen, Phys. Rev. B 5 (1972) 3058.
[12] J.R. Chelikowsky, M.L. Cohen, Phys. Rev. B 14 (1976) 556.
[13] A. Zunger, A.J. Freeman, Phys. Rev. B 17 (1978) 4850.
[14] K.J. Chang, S. Froyen, M.L. Cohen, Phys. Rev. B 28 (1983) 4736.
[15] M.Z. Huang, W.Y. Ching, J. Phys. Chem. Solids 46 (1985) 977.
[16] Ali Hussain Reshak, J. Chem. Phys. 124 (2006) 104707.
[17] G.K.H. Madsen, P. Blaha, K. Schwarz, E. Sjöstedt, L. Nordström, Phys. Rev. B 64 (2001) 195134.
[18] K. Schwarz, P. Blaha, G.K.H. Madsen, Comput. Phys. Commun. 147 (2002) 71.
[19] P. Blaha, K. Schwarz, G.K.H. Madsen, D. Kvasnicka, J. Luitz, Computer Code wien2k, An Augmented Plane Wave Plus Local Orbitals Program for Calculating Crystal Properties, Vienna University of Technology, Vienna, Austria, 2001, ISBN 3-9501031-1-2.
[20] A. Zunger, S.-H. Wei, L.G. Feireira, J.E. Bernard, Phys. Rev. Lett. 65 (1990) 353.
[21] J.P. Perdew, K. Burke, M. Ernzerhof, Phys. Rev. Lett. 77 (1996) 3865.
[22] E. Engel, S.H. Vosko, Phys. Phys. Rev. B 47 (1993) 13164.
[23] P. Dufek, P. Blaha, K. Schwarz, Phys. Rev. B 50 (1994) 7279.
[24] P.E. Blöchl, O. Jepsen, O.K. Anderson, Phys. Rev. B 49 (1994) 16223.
[25] F.D. Murnaghan, Proc. Natl. Acad. Sci. U. S. A. 30 (1944) 244.
[26] M.-Z. Huang, W.Y. Ching, Phys. Rev. B 47 (1993) 9449.
[27] A.H. Reshak, R. Khenata, I.V. Kityk, K.J. Plucinski, S. Auluck, J. Phys. Chem. 113 (2009) 5803.
[28] S.N. Rashkeev, W.R.L. Lambrecht, B. Segall, Phys. Rev. B 57 (1998) 3905.
[29] S.N. Rashkeev, W.R.L. Lambrecht, B. Segall, Phys. Rev. B 57 (1998) 9705.
[30] H.Z. Tributsch, Naturforsch A 32A (1977) 972.
[31] D.R. Penn, Phys. Rev. 128 (1962) 2093.
[32] A.H. Reshak, Ph.D. Thesis, Indian Institute of Technology-Roorkee-India, 2005.
[33] S. Sharma, C. Ambrosch-Draxl, Phys. Scripta T 109 (2004) 128.
[34] S. Sharma, J.K. Dewhurst, C. Ambrosch-Draxl, Phys. Rev. B 67 (2003) 165332.
[35] J.L.P. Hughes, J.E. Sipe, Phys. Rev. B 53 (1996) 10751.
[36] S.N. Rashkeev, W.R.L. Lambrecht, Phys. Rev. B 63 (2001) 165212.
[37] R.W.G. Wyckoff (Ed.), Crystal Structures, vol. 1, John Wiley & Sons, Inc., 1963.
[38] L. Ley, R.A. Pollak, F.R. McFeely, S.P. Kowalczyk, D.A. Shirley, Phys. Rev. B 9 (1974) 600.
[39] K.O. Magnusson, U.O. Karlsson, D. Straub, S.A. Flodström, F.J. Himpsel, Phys. Rev. B 36 (1987) 6566.
[40] T.K. Bergstresser, M.L. Cohen, Phys. Rev. 164 (1967) 1069.
[41] A. Kobayashi, O.F. Sankey, S.M. Volz, J.D. Dow, Phys. Rev. B 28 (1983) 935.
[42] D.J. Stukel, R.N. Euwema, T.C. Collins, F. Herman, R.L. Kortum, Phys. Rev. 179 (1969) 740.
[43] J.L. Freeouf, Phys. Rev. B 7 (1973) 3810.
[44] A. Manabe, A. Mitsuishi, H. Yoshinaga, Jpn. J. Appl. Phys. 6 (1967) 593.
[45] D.T.F. Marple, J. Appl. Phys. 35 (1964) 539.
[46] R.A. Soref, H.W. Moos, J. Appl. Phys. 188 (1969) 1211.
[47] C.K.N. Patel, Phys. Rev. Lett. 16 (1966) 613.
[48] M.M. Choy, R.L. Byer, Phys. Rev. B 14 (1976) 1693.
[49] G.H. Sherman, P.D. Coleman, J. Appl. Phys. 44 (1973) 238.
[50] B.F. Levine, Phys. Rev. B 7 (1973) 2600.
[51] J.C. Phillips, J.A. Van Vechter, Phys. Rev. 183 (1969) 709.
[52] D.A. Kleinman, Phys. Rev. B 2 (1970) 3139.
[53] C.L. Tang, C. Flytzanis, Phys. Rev. B 4 (1971) 2520.
[54] M.I. Bell, Phys. Rev. B 6 (1972) 516.
[55] C.L. Tang, IEEE J. Quantum Electron. QE-9 (1973) 755.
[56] D.E. Aspnes, Phys. Rev. B 6 (1972) 4648.
[57] M.M. Choy, S. Ciraci, R.L. Byer, IEEE J. Quantum Electron. QE-11 (1975) 40.
[58] E. Ghahramani, D.J. Moss, J.E. Sipe, Phys. Rev. B 43 (1991) 9700;
E. Ghahramani, D.J. Moss, J.E. Sipe, Phys. Rev. B 43 (1991) 8990.
[59] O. Madelung, M. Schlz, H. Weiss, Landolt-Borstein, Numerical Data and Functional Relationships in Science and Technology, vol. 17, Springer, Berlin, 1982.
[60] J. Heyd, J.E. Peralta, G.E. Scuseria, J. Chem. Phys. 123 (2005) 174101.

[61] E. Deligoz, K. Colakoglu, Y. Ciftci, Physica B 373 (2006) 124.
[62] S. Zerroug, F. Ali Sahraoui, N. Bouarissa, Eur. Phys. J. B 57 (2007) 9.
[63] Z.C. Feng, P. Becla, L.S. Kim, S. Perkowitz, Y.P. Feng, H.C. Poon, K.P. Williams, G.D. Pitt, J. Cryst. Growth 138 (1994) 239.
[64] J.P. Mangalhara, R. Thangaraj, O.P. Agnihotrii, Solar Energy Mater. 19 (1989) 157.
[65] H.C. Poon, J. Phys. Condens. Matter 7 (1995) 2783.
[66] S.M. Hosseini, Physica B 403 (2008) 1907.